Remote Sensing of Environment 127 (2012) 60–73

Contents lists available at SciVerse ScienceDirect

Remote Sensing of Environment

journal homepage: www.elsevier.com/locate/rse

A comparison of forest cover maps in Mainland Southeast Asia from multiple sources: PALSAR, MERIS, MODIS and FRA

Jinwei Dong [a,*], Xiangming Xiao [a], Sage Sheldon [a], Chandrashekhar Biradar [a], Nguyen Dinh Duong [b], Manzul Hazarika [c]

[a] Department of Microbiology and Plant Botany, and Center for Spatial Analysis, University of Oklahoma, Norman, OK 73019, USA
[b] Institute of Geography, Vietnam Academy of Science and Technology, 18 Hoang Quoc Viet Rd., Cau Giay, Hanoi, Vietnam
[c] Geoinformatics Center, Asian Institute of Technology, P.O. Klong Luang, Pathumthani 12120, Thailand

ARTICLE INFO

Article history:
Received 20 January 2012
Received in revised form 14 August 2012
Accepted 19 August 2012
Available online 18 September 2012

Keywords:
Forest mapping
Southeast Asia
PALSAR
MCD12Q1
GlobCover
FRA

ABSTRACT

The uncertainty in tracking tropical forest extent and changes substantially affects our assessment of the consequences of forest change on the global carbon cycle, biodiversity and ecosystem services. Recently cloud-free imagery useful for tropical forest mapping from the Phased Array Type L-band Synthetic Aperture Radar (PALSAR) onboard the Advanced Land Observing Satellite (ALOS) has become available. We used PALSAR 50-m orthorectified mosaic imagery in 2009 and a decision tree method to conduct land cover classification and generate a 2009 forest map, which was evaluated using 2106 field photos from the Global Geo-referenced Field Photo Library (http://www.eomf.ou.edu/photos). The resulting land cover classification had a high overall accuracy of 93.3% and a Kappa Coefficient of 0.9. The PALSAR-based forest map was then compared with three existing forest cover products at three scales (regional, national, and continental): the Food and Agriculture Organization of the United Nations (FAO) Forest Resources Assessments (FRA) 2010, Global Land Cover Map with MERIS (GlobCover) 2009, and the MODIS Terra + Aqua Land Cover Type product (MCD12Q1) 2009. The intercomparison results show that these four forest datasets differ. The PALSAR-based forest area estimate is within the range ($6.1–9.0\times10^5$ km^2) of the other three products and closest to the FAO FRA 2010 estimate. The spatial disagreements of the PALSAR-based forest, MCD12Q1 forest and GlobCover forest are evident; however, the PALSAR-based forest map provides more details (50-m spatial resolution) and high accuracy (the Producer's and the User's Accuracies were 88% and 95%, respectively) and PALSAR can be used to evaluate MCD12Q1 2009 and GlobCover 2009 forest maps. Given the higher spatial resolution, PALSAR-based forest products could further improve the modeling accuracy of carbon cycle in tropical forests.

1. Introduction

Large-scale deforestation in tropical regions has attracted much attention in the past few decades due to its strong effects on atmospheric greenhouse gases (Fearnside, 2000), biodiversity (Lawton et al., 1998; Pimm & Raven, 2000), and regional climate (Salati & Nobre, 1991). Forest management requires timely and accurate information on forests (Hansen et al., 2008).

Southeast Asia has the third largest area of tropical rainforest in the world, which is composed of tropical evergreen forest and deciduous forest in seasonal drought areas. However, it has been experiencing a more significant deforestation for conversion into agriculture (such as oil palm plantations) than anywhere else (UNEP/GRID-Arendal, 2009). The humid tropical forest cover in Southeast Asia underwent the largest changes with an annual net cover decrease rate of 0.71% from 1990 to 1997, higher than Latin America and Africa (Achard et al., 2002). Much attention has been focused on those hotspots of deforestation, including Borneo (Curran, 2004; Langner et al., 2007; Meijaard & Sheil, 2007; Miettinen, 2007) and Sulawesi (Dechert et al., 2004). An accurate forest map is essential for efforts in 'reducing emissions from deforestation and forest degradation' (REDD).

Remote sensing has been used for forest inventory for decades (Hansen et al., 2010a, 2010b, 2008) and is considered to be an effective tool for detecting forest extents and changes at regional and global scales. A number of studies have sought to map forests in Southeast Asia using a remote sensing approach. For example, the National Oceanic and Atmospheric Administration Advanced Very High Resolution Radiometer (NOAA/AVHRR) data of 1990–1992 was used to map forests through unsupervised classification of a vegetation index (Normalized Difference Vegetation Index, NDVI) and Channel 3 radiance (Achard & Estreguil, 1995). However, its accuracy could

* Corresponding author at: Department of Microbiology and Plant Botany, and Center for Spatial Analysis, University of Oklahoma, 101 David L. Boren Blvd. Norman, OK 73019, USA. Tel.: +1 405 325 6091.
E-mail address: jinwei.dong@ou.edu (J. Dong).

0034-4257/$ – see front matter © 2012 Elsevier Inc. All rights reserved.
http://dx.doi.org/10.1016/j.rse.2012.08.022

be misleading in both its thematic legend and statistical data as there was no accuracy assessment due to technical limitations (Achard et al., 2001). Imagery from the SPOT-Vegetation sensor over the period of 1998–2000 was also used to map tropical forest cover in Insular Southeast Asia (Stibig & Malingreau, 2003; Stibig et al., 2004). Recently, imagery from the Moderate Resolution Imaging Spectroradiometer (MODIS) has been widely used for forest cover mapping (Langner et al., 2007; Tottrup et al., 2007; Xiao et al., 2009). However, estimates of tropical forest area and deforestation rates based on optical remote sensing are still uncertain due to frequent cloud coverage (Agrawal et al., 2008; Chazdon, 2008; Grainger, 2008; Wurster et al., 2010).

A review of previous studies (Table 1) allows for estimating the rates of deforestation in Southeast Asia during the past few decades. According to Achard et al. (2002), an annual deforestation rate of 0.91% occurred in Southeast Asia during 1990–1997, determined by utilizing a stratified systematic sampling scheme with 100 sample sites covering 6.5% of the humid tropical domain. A decrease of deforestation in Southeast Asia was reported in the Food and Agriculture Organization of the United Nations (FAO) Forest Resources Assessments (FRA) 2010 (FAO, 2010); however, the deforestation was not spatially homogeneous. Miettinen et al. (2011) found that from 2000 to 2010 deforestation continued with an annual rate of 1.0% in Insular Southeast Asia, according to an investigation based on MODIS data at 250-m spatial resolution. It remains unclear what has happened to the forests in Mainland Southeast Asia (MSEA) in recent years. Also, the forest trend reliability was uncertain due to inconsistencies between study periods or different data sources (Fritz et al., 2011; Grainger, 2010). Improved and dynamic forest cover monitoring is needed in order to produce a more reliable trend analysis.

Given the limitation of optical remote sensing in tropical forest mapping, cloud-free synthetic aperture radar (SAR) has the potential to be an important data source for forest mapping. Previous studies showed that a longer radar wavelength (e.g. L-band SAR) is more suitable to the delineation of forest than shorter wavelengths because of its greater penetration through the tree canopy (Baghdadi et al., 2009). The Phased Array Type L-band Synthetic Aperture Radar (PALSAR) onboard the Advanced Land Observing Satellite (ALOS) was launched by the Japan Aerospace Exploration Agency (JAXA) in January of 2006 and provided polarimetric radar images for the global land surface that have been used for forest mapping (Almeida et al., 2009; Santoro et al., 2010; Xiao et al., 2010). Studies in Insular Southeast Asia have shown the potential of PALSAR imagery for regional forest monitoring (Longepe et al., 2011; Miettinen & Liew, 2011; Walker et al., 2010). JAXA has generated the world's first global forest and non-forest area distribution (in 2007 and 2009) with a 10-meter resolution, by using ALOS/PALSAR data. However, the 10-m forest/non-forest map is still unavailable to the public, yet (JAXA-EORC, 2010). In addition, the Woods Hole Research Center is developing a pan-tropical forest cover map as baseline data for subsequent deforestation and forest degradation monitoring by using a pan-tropical database of high-resolution ALOS/PALSAR data (Kellndorfer, 2010). To support regional-scale studies, JAXA released the PALSAR 50-m orthorectified mosaic imagery (fine bean with dual polarization) in 2007, 2008 and 2009 for many parts of the world and MSEA has good PALSAR 50-m data coverage.

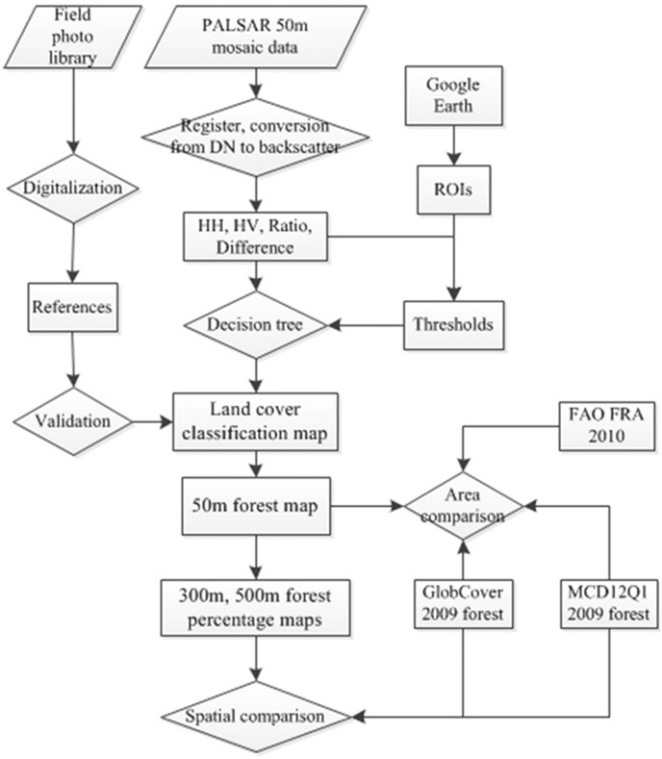

Fig. 1. The workflow for mapping tropical forests based on PALSAR 50-m orthorectified mosaic imagery. PALSAR 50-m mosaic was used as the imagery data source, and decision tree method was applied together with training and validation reference data from the Global Geo-Referenced Field Photo Library and Google Earth. Three existing global forest datasets (300-m Globcover in 2009, 500-m MCD12Q1 in 2009, and statistical FAO FRA 2010 report) were used for comparison.

The objective of this study is twofold: (1) to generate an accurate map of tropical forest in MSEA based on the ALOS/PALSAR 50-m orthorectified mosaic products in 2009, and (2) to compare the PALSAR-based forest map with FAO FRA 2010 and two forest maps generated from moderate resolution imagery (MODIS and MERIS), which will help understand the error and uncertainty of these three datasets (Fig. 1). The results from this study will support forest inventory and management.

2. Data and methods

Southeast Asia geographically includes a mainland area and a string of archipelagoes to the south and east. It is commonly divided into two sub-regions: MSEA (or Indochina) and Insular Southeast Asia (or Maritime Southeast Asia). MSEA includes five countries (Cambodia, Laos, Myanmar, Thailand, Vietnam) and Peninsular Malaysia; Insular Southeast Asia includes East Malaysia and five countries (Brunei, Indonesia, Philippines, Singapore, and East Timor). In this study, we focused on the main body of MSEA, that is, Vietnam, Laos, Cambodia, Thailand and Myanmar. The elevation is very high in the northern parts of the study area and low and smooth

Table 1
A summary about existing tropical forest maps in Southeast Asia (SEA).

References	Regions	Study period	Data sources	Validation and Accuracy
(Achard & Estreguil, 1995)	SEA	1990–1992	AVHRR	Existing vegetation maps and TM
(Stibig et al., 2004)	Mainland SEA	1998–2000	SPOT4-vegetation	TM and FAO FRA
(Giri et al., 2003)	Mainland SEA	1985/86, 1992	AVHRR	Field surveys in hotpots
(Stibig & Malingreau, 2003)	Insular SEA	1998–2000	SPOT4-vegetation	Existing forest data and FAO data
(Miettinen et al., 2012)	Insular SEA	2010	MODIS, PALSAR 50 m mosaic	TM and IKONOS
(Achard et al., 2001)	Pan-tropical forest belt	Early 1990s	AVHRR	TM

in southern parts of Myanmar, Thailand, Cambodia, and eastern Vietnam (Fig. 2).

MSEA belongs to the warm and humid tropics; however, climate is variable inside the region due to the complex topography. Coastal areas have a tropical humid climate. Most interior regions of MSEA (particularly the Khorat Plateau in the northern Myanmar, Laos, and northern Vietnam) are characterized as monsoon climate with distinct wet and dry seasons. The winter northeast monsoon occurs roughly from November to March and brings relatively dry, cool air and little precipitation, while the summer southwest monsoon prevails from May to September and brings a large amount of precipitation during the wet season to the mainland.

2.1. PALSAR 50-m orthorectified mosaic imagery

The PALSAR 50-m orthorectified mosaic data, provided by JAXA, is created globally with images in the ascending path. The original PALSAR images have an off-nadir angle of 34.3° and cover dry and wet seasons, or summer and winter seasons, and were resampled into the 50-m by 50-m mosaic to create one composite per year. The dates of image acquisition vary between years. It has been geometrically rectified using a 90-m digital elevation model (DEM) and geo-referenced into geographical latitude and longitude coordinates (Longepe et al., 2011). The mosaic algorithm including calibration and validation of PALSAR 50-m orthorectified mosaic product has been reported in (Shimada & Ohtaki, 2010; Shimada et al., 2008). These PALSAR 50-m mosaic data are freely available to the public at the ALOS Kyoto and Carbon Initiative official website (http://www.eorc.jaxa.jp/ALOS/en/kc_mosaic/kc_mosaic.htm). For this study, we downloaded the PALSAR 50-m orthorectified mosaic product with the Fine Beam Dual polarization (FBD) observational mode from July to Oct. 2009, which has two polarizations: HH and HV. HH means microwave energy was both transmitted and received in the horizontal direction by the radar antenna, while HV means microwave energy transmitted in the horizontal direction and received in the vertical direction. The Digital Number (DN) values (amplitude values) were converted into normalized radar cross section in decibel (dB) according to the formula from JAXA (Rosenqvist et al., 2007) and the parameters from the metadata of each file:

$$\sigma^0(dB) = 10 \times \log_{10} DN^2 + CF \quad (1)$$

where σ^0 is the backscattering coefficient, *DN* is the digital number value of pixels in HH or HV; and *CF* is the absolute calibration factor of −83.

We produced two additional images: (1) the ratio image of HH and HV (Ratio = HH/HV) and (2) the difference image between HH and HV (Difference = HH − HV). These two composited images proved valuable for land cover classification (Miettinen & Liew, 2011; Wu et al., 2011). Visual image evaluation shows that the difference image is less affected by shadows due to complex topography than does the ratio image. The difference image (HH-HV) was also used in previous studies for land cover mapping (Longepe et al., 2011; Walker et al., 2010). A color composite map from HH, HV and

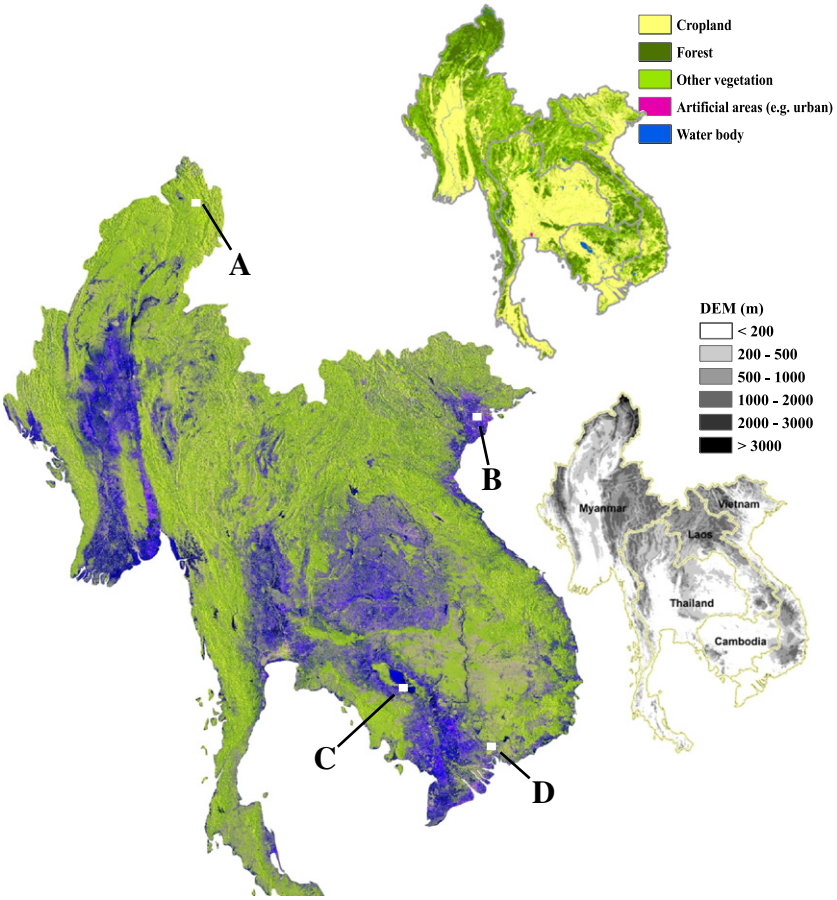

Fig. 2. Color composite map of PALSAR polarizations (R, G, B = HH, HV, and Difference, respectively). Image Data© JAXA, METI. Two small maps show the land cover distribution from GlobCover 2009 and topography from 90-m digital elevation data. The subsets (white boxes A, B, C and D) for four land covers (shown in Fig. 4) show that PALSAR has good performances in identifying forest, cropland, water and buildings.

Difference images showed a visual separability of land-cover types in the region (Fig. 2).

2.2. Extraction of regions of interest (ROIs) from the Global Geo-Referenced Field Photo Library and Google Earth

Ground truth samples, which are used as training data for supervised classification or validation data for accuracy assessment, are important for land cover classification. We used the geo-referenced field photos in the Global Geo-Referenced Field Photo Library at the University of Oklahoma (http://www.eomf.ou.edu/photos/), a citizen science data portal for archive, sharing and exchange of geo-tagged field photos and associated thematic databases of land cover types from the individual photos (Xiao et al., 2011). The geo-tagged field photos in the Field Photo Library come from researchers and citizens with GPS cameras and smartphones, and many of the field photos were also described with detailed information on land cover types, e.g., forests, rubber plantation, paddy rice, winter wheat, sugarcane, and so on. Field photos have been a part of field surveys for decades, and this citizen-based Field Photo Library provides a web-based venue for researchers and citizens to share their ground reference data and make it available to the public. The geo-referenced field photos can be easily uploaded to the website and downloaded into different formats, e.g., Keyhole Markup Language files (.kml or .kmz), ArcGIS vector files (shapefile), and dbf format files. In this study, a total of 2106 geo-referenced field photos from Thailand, Vietnam, and Myanmar were used (Fig. 3B); of which, 2052 were from our field trips in Thailand and Vietnam, 54 in Myanmar, Cambodia and Laos were from the Degree Confluence Project (http://confluence.org/).

We also used Google Earth to locate and digitize ROIs, as it has very high spatial resolution imagery, particularly in the regions around cities. A previous study showed that Google Earth's High-Resolution Imagery Archive has high horizontal positional accuracy (Potere, 2008). Several studies have used Google Earth to collect validation information for land cover classification (Benedek & Sziranyi, 2009; Cohen et al., 2010; Gemmell et al., 2009; Montesano et al., 2009). In this study, a series of random sampling points were generated with Google Earth high-resolution images as reference and interpreted into ROIs for signature analysis and decision tree rule training. The samples were selected inside large patches with intact land cover; thus, all ROIs were extracted for locations where only a single land cover type covered the area. Finally, 1.4×10^7 PALSAR pixels were acquired from the ROIs defined by Google Earth, including 997 986 forest pixels (25 ROIs), 160 916 cropland pixels (32 ROIs), 303 948 water pixels (10 ROIs), and 26 970 built-up land pixels (11 ROIs), which covered ~2% of all pixels in the study area (there are 807.6 million pixels covering the study area). All pixels were used for determining the rules of decision tree (Fig. 3A).

In addition, all field-photo-located points were used as references to digitalize ROIs in Google Earth and land cover classification validation was done with these ROIs. Four land cover types of ROIs were digitalized and acquired according to the field-photos in Google Earth (Fig. 3B). As our field photos were mainly for forest and cropland, water and built-up land were acquired directly in Google Earth. Built-up land is quite easy to identify due to higher spatial resolution imagery in urban areas, as is water body due to its color.

2.3. Analysis of PALSAR backscatter signatures for land cover types

The radar backscatter is affected by many complex factors, including frequency, polarization, surface roughness, geometric shape (e.g. inclination of land surface) and dielectric properties of the target, and so on. L-band PALSAR has a more powerful canopy penetrating ability than C and X-bands (Baghdadi et al., 2009),

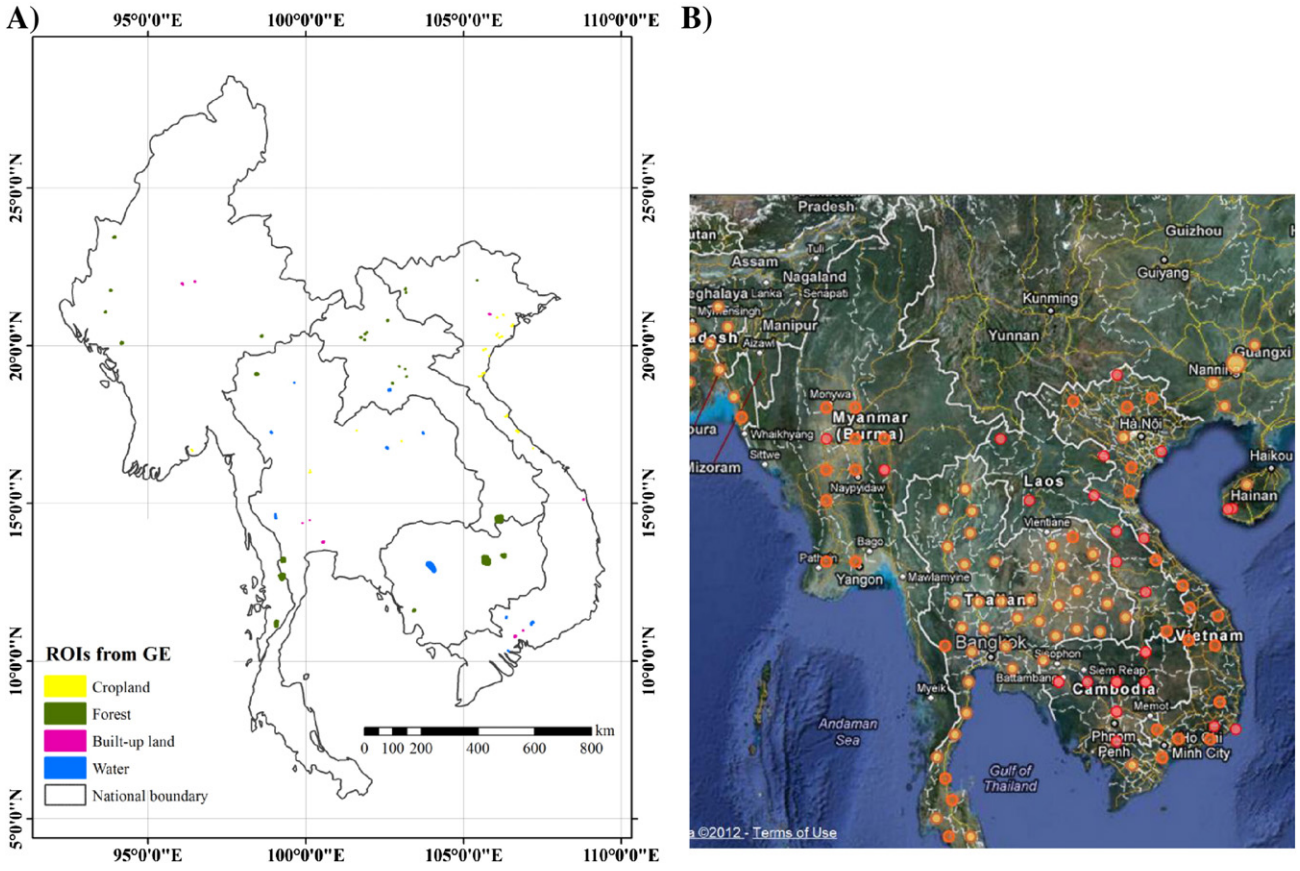

Fig. 3. Spatial distributions of A) ROIs used for training analysis from Google Earth, and B) field photo locations for validation (http://www.eomf.ou.edu/photos/).

therefore, the size and form of trunks, branches and leaves affects the backscatter of L-band.

We calculated the frequency distributions of the two polarizations (HH and HV), the Ratio image and the Difference image for four land-cover types. The histogram of the HH image (Fig. 4A) shows that water has much lower backscatter values than forests and partly overlapped with cropland; as inland water bodies tend to be relatively calm and smooth, reflecting most of the backscatter in directions other than the sensor. This means water is separable from forests, urban areas and most cropland. Both forests and urban areas have high HH backscatter values, and some urban areas (most likely large building complex) have even higher backscatter values than forests due to the complex reflectance environments caused by building orientations and corner reflectors. There is some degree of overlap in HH backscatter among forests, buildings and cropland. The histogram of the HV image (Fig. 4B) shows that forests have higher HV values than water and cropland due to depolarization caused by complex structure (tree trunks and leaf canopy) and a large amount of biomass. The HV histogram of forests only slightly overlaps with that of cropland and has relatively more overlaps with built-up land as large patches of forests distributed in urban areas. Therefore, HV is a good indicator for separating forests from water and cropland, but not sufficient for complete separation of forests and built-up land. The histogram of the Ratio image (Fig. 4C) shows that all three land cover types have an overlapping range with forests for this indicator. The histogram of the Difference image (Fig. 4D) shows that forest has very low values, while cropland has relative high values.

2.4. PALSAR threshold values and decision tree method for mapping forests

The above exploratory data analysis (Section 2.3) provides useful information for constructing a decision tree algorithm based on the threshold values from the HH, HV, HH/HV and HH–HV images. First, water can be delineated easily as it has very low HH and HV values. Secondly, forests tend to have higher HH and HV values, and lower Difference values, although build-up lands partly overlapped with forest. Cropland can also be distinguished and mapped.

Here we used the 95% confidence interval of the previously discussed histograms of individual images (HH, HV, HH/HV, and

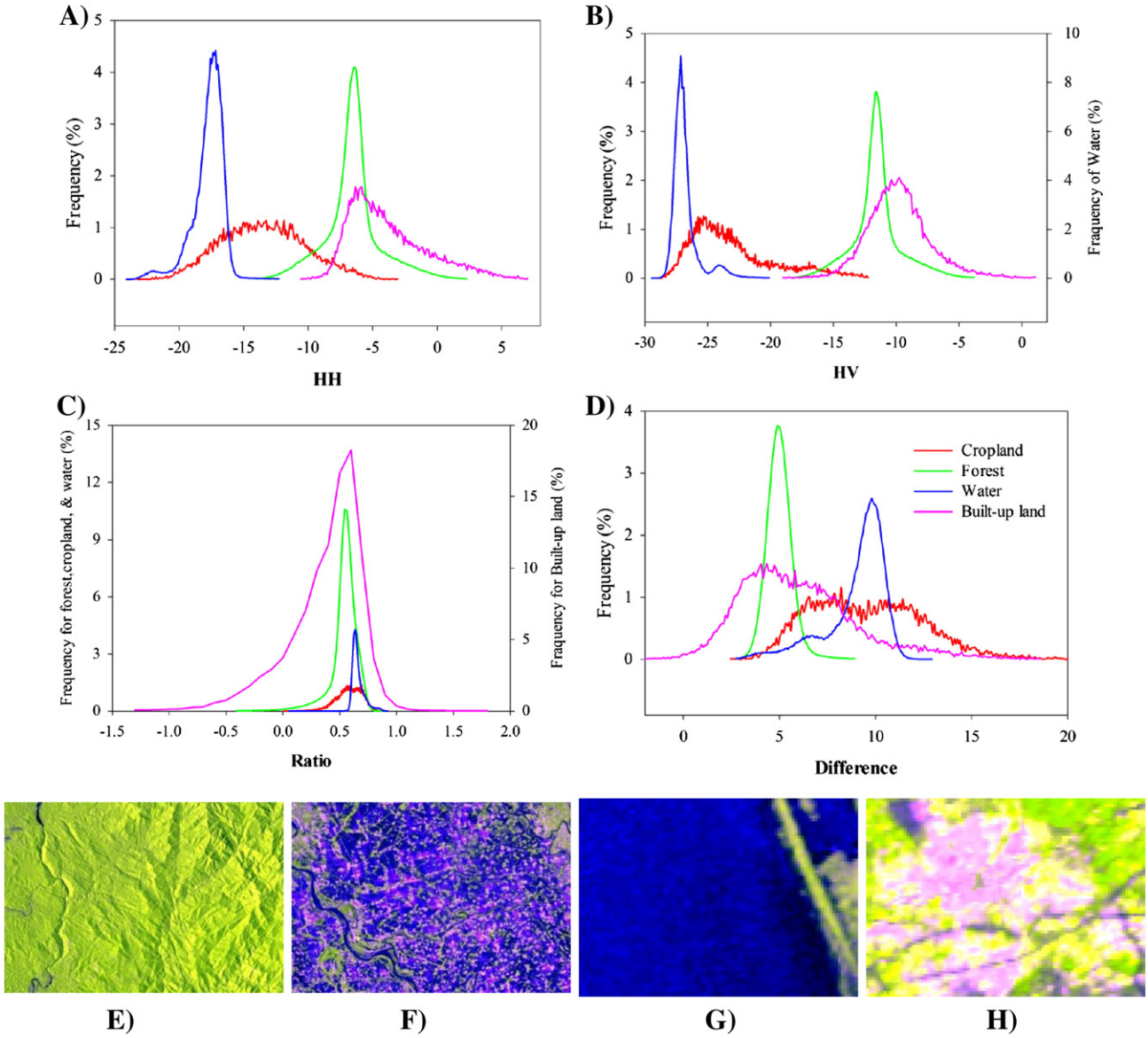

Fig. 4. The backscatter signatures of different land covers in four images. A) HH polarization, B) HV polarization, C) Ratio image (HH/HV), and D) Difference image (HH–HV). The samples in this figure were extracted from PALSAR 2009 data. Four subsets from the color composition map (corresponding with A, B, C and D in Fig. 2) showed four land covers including E) forest, F) cropland (mixed with some residential land), G) water and H) buildings.

HH–HV) to define threshold values for decision tree rules (Fig. 4). We assume that the ROIs of individual land cover types have some uncertainty and we exclude 2.5% pixels with lowest and highest backscatter values, respectively. The threshold values were further rounded to integer number for HH and HV, and to 0.5 decimal unit for ratio and difference images. We selected the following threshold values for the decision tree rules:

If HH<−16 and HV<−24 then a pixel is classified as water;
Else if 3.5<Difference<6.5 and −15<HV<−7 and 0.3<Ratio<0.7 then a pixel is classified as forest;
Else if HV<−16 then a pixel is classified as cropland;
Else a pixel is labeled as other land cover or un-classified.

These threshold values for the decision tree algorithm are based on the PALSAR images in 2009. As with all supervised classification approaches, these threshold values are unique for PALSAR images in 2009 and MSEA, and might not apply to PALSAR images acquired in other regions or periods without careful examination of PALSAR imagery used. The decision tree was built and executed in ENVI 4.8 software and the resulting 50-m land cover map is shown in Fig. 5. The forest class was extracted to generate a forest map at 50-m resolution in 2009. We aggregated the 50-m forest map and calculated forest percentage within 300-m pixels and 500-m pixels (Fig. 8), and the resulting fractional forest maps at 300-m and 500-m resolutions are used to compare with forest maps from the GlobCover 2009 dataset (300-m resolution) and the MCD12Q1 2009 dataset (500-m resolution).

2.5. Validation of PALSAR-based forest map in 2009

The accuracy of the PALSAR-based forest map was assessed by using samples interpreted from 2106 field photos in MSEA (see Section 2.2 for detailed sample acquirement approach). 98 320 pixels were used for the validation of land cover classification, including 28 054 forest pixels, 8,965 cropland pixels, 50 617 water pixels, and 10 684 built-up land pixels (Table 2). The accuracy assessment was performed by using the "Ground Truth ROIs" method in ENVI software. In addition, we displayed the resulting maps of individual land cover types in the image windows of the ENVI software, which is linked with Google Earth, and carried out visual evaluation of the maps.

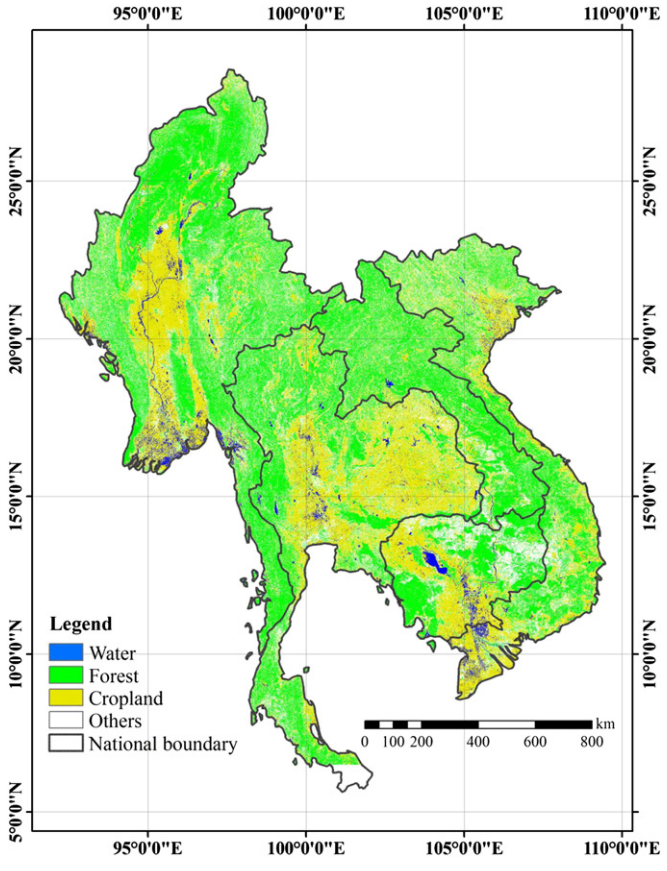

Fig. 5. The land-cover classification result based on the decision tree method and PALSAR 50-m orthorectified mosaic imagery in 2009.

2.6. Comparison with existing land cover products

Several regional and global forest maps have been generated from optical sensors, including a MODIS-based global land cover map (Friedl et al., 2010) and a MERIS-based global land cover map (Bontemps et al., 2011). Limited effort has been devoted to evaluation of these forest maps due to lack of resources (Kaptue Tchuente et al., 2011). We compared the PALSAR-based forest map with the following three forest data products that are widely used:

FAO FRA 2010 forest area data. FAO has monitored and reported the world's forests at 5–10 year intervals since 1946. The FAO FRA 2010 is the most comprehensive forest assessment to date. Forest area estimates were collected from cooperating member countries; FRA 2010 covered 233 countries, which increased from 212 in FRA 2000. The original data, data reliability indications, and terminology definitions from all the member countries were collected, a series of processes were conducted (e.g., reclassification of national data into the FRA classification system), and internal consistency checks were performed (FAO, 2010). The national statistical table was used in this study. FAO has initiated a new satellite-based survey, and initial results were released in 2011, reporting forest change from 1990 to 2005 (FAO et al., 2009). However, this new high resolution remote sensing survey is currently unavailable to the public.

The GlobCover 2009 land cover product was generated by the GlobCover project under the support of the European Space Agency. GlobCover 2009 is a 300-m global land cover product based on MERIS FR time series data from Jan to Dec 2009 collected onboard the ENVISAT satellite (Bontemps et al., 2011), available at its official website (http://ionia1.esrin.esa.int/index.asp). It is composed of 22 different land cover types, including seven forest dominated types (Table 3). In this study, we combined them into one forest layer and compared the resultant forest map with the PALSAR-based forest map.

The MODIS MCD12Q1 land cover product was generated by the MODIS Land Science Team, using MODIS 500-m surface reflectance data from Terra and Aqua platforms (Friedl et al., 2010). The MCD12Q1 (the MODIS Terra + Aqua Land Cover Type Yearly L3 Global 500 m SIN Grid product) data product has several land cover

Table 2
Confusion matrix between PALSAR-based land cover classification and ground truth samples from field photos. The land cover of "others" means urban land and other land covers.

	Class	Ground truth samples (pixels)				Total classified pixels	User Acc. (%)
		Water	Others	Forest	Cropland		
Classification	Water	49735	0	0	563	50298	99%
	Others	9	9327	2784	396	12516	75%
	Forest	16	1328	24746	54	26144	95%
	Cropland	857	29	524	7952	9362	85%
Total ground truth pixels		50617	10684	28054	8965	98320	
Prod. Acc. (%)		98%	87%	88%	89%		

Table 3
The land-cover types of MCD12Q1 and GlobCover that was combined into the forest domain in this study.

Forest category from GlobCover	Forest category from MCD12Q1
Closed to open (>15%) broadleaved evergreen or semi-deciduous forest (>5 m)	Evergreen needleleaf forest Evergreen broadleaf forest
Closed (>40%) broadleaved deciduous forest (>5 m)	Deciduous needleleaf forest
Open (15–40%) broadleaved deciduous forest/woodland (>5 m)	Deciduous broadleaf forest
Closed (>40%) needleleaved evergreen forest (>5 m)	Mixed forest
Open (15–40%) needleleaved deciduous or evergreen forest (>5 m)	
Closed to open (>15%) mixed broadleaved and needleleaved forest (>5 m)	
Mosaic forest or shrubland (50–70%) / grassland (20–50%)	
Closed to open (>15%) broadleaved forest regularly flooded (semi-permanently or temporarily) — Fresh or brackish water	

classification schemes, and we used the primary land cover scheme from the International Geosphere Biosphere Programme (IGBP), which includes 17 land cover classes. Five forest types (Evergreen Needleleaf forest, Evergreen Broadleaf forest, Deciduous Needleleaf forest, Deciduous Broadleaf forest, and Mixed forest) were combined into one forest layer for comparison with the PALSAR-based forest map.

3. Results

3.1. Forest map of Mainland Southeast Asia from 2009 PALSAR 50-m orthorectified mosaic imagery

The PALSAR-based algorithm estimates a forest area of 8.7×10^5 km^2 in MSEA (five countries), which covered 46% of the land area in the region. Fig. 5 shows the spatial distribution of this forest estimate in MSEA. Ground reference points, derived from digitalization in Google Earth referring to the Global Geo-Referenced Field Photo Library, were adopted to evaluate the accuracy of the land cover classification. 98 320 pixels from 532 ROIs were used to assess the accuracy of the PALSAR land cover map at 50-m resolution. The results showed that the land cover classification had an overall accuracy of 93.3% and a Kappa Coefficient of 0.9. The Producer's Accuracy and the User's Accuracy of forest were 88% and 95%, respectively (Table 2). Water has the highest accuracy in both the Producer's Accuracy and the User's Accuracy because of its extremely low HH and HV values. The User's and Producer's Accuracy of cropland were also high (85 % and 89 %, respectively). In general, the decision tree based classification had a reasonably high accuracy for mapping forest in the region.

3.2. Area comparison between PALSAR-based forest map and other three forest cover products

At the continental scale, forest proportion is high in MSEA according to FRA 2010, accounting for over 48% of land area in the five countries (FAO, 2010). Among the three existing land cover datasets (FRA 2010, GlobCover 2009, and MCD12Q1 2009), forest area estimates in MSEA range from 6.1×10^5 km^2 (GlobCover 2009) to 9.0×10^5 km^2 (FRA 2010), which suggests a large uncertainty in estimating forest area in the region. Our PALSAR-based forest area estimate (8.7×10^5 km^2) was within the range of the other three forest datasets, but most consistent with the estimate of FRA 2010.

At the country scale, Myanmar has the largest amount of forest area among five countries (Fig. 6), and the forest area estimate in Myanmar from GlobCover 2009 is substantially lower than those from PALSAR 2009, FRA 2010 and MCD12Q1-2009. In Thailand, forest area estimates from MCD12Q1-2009 and GlobCover 2009 were substantially lower than those from FRA 2010 and PALSAR 2009. In Vietnam, forest area estimates from the four datasets have relatively small differences between them. Forest area estimate from the FRA 2010 is slightly larger than that from PALSAR 2009 in Cambodia, Laos, Thailand and Vietnam, while forest estimate in Myanmar from PALSAR 2009 is higher than that from FRA 2010.

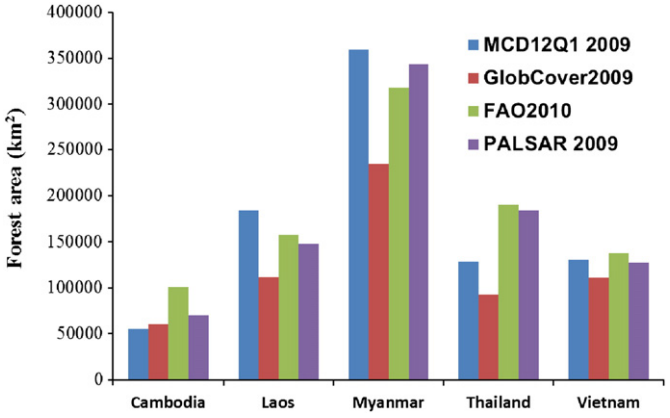

Fig. 6. A comparison of forest area estimates (unit: km^2) in Mainland Southeast Asia among four datasets: PALSAR 2009, MCD12Q1 2009, GlobCover 2009 and FAO FRA 2010.

At the pixel level, Fig. 7 shows the spatial distribution of forest from three datasets (PALSAR 2009, GlobCover 2009 and MCD12Q1 2009). Visually it seems that all the three products have some degree of spatial consistency for most of the study area. However, there is a relatively large difference between these maps, e. g., in the middle-eastern region of Myanmar (the blue circle in Fig. 7), where PALSAR 2009 showed more forest area, but both MCD12Q1 2009 and GlobCover 2009 show a small area of forest. Comparison with Google Earth images in multiple locations in Myanmar shows that a large area of forest was indeed present. This indicates that PALSAR imagery has a stronger and improved capacity to map forest, which may be partially attributed to the higher spatial resolution of PALSAR and the nature of radar data. Subset comparisons using Google Earth as reference data clearly illustrate the potential of PALSAR 50-m orthorectified mosaic imagery in improving forest mapping when compared with moderate resolution imagery (MERIS and MODIS).

3.3. Spatial intercomparison of forest cover maps: PALSAR, MERIS, and MODIS

In order to compare the three datasets at the same spatial resolution, these three forest cover maps were first aggregated into forest percentage maps with a 1500-m resolution (the least common multiple of the three spatial resolutions — 50-m, 300-m, 500-m), and then the piecewise disagreement analysis between them was conducted by using the difference of two forest percentage maps. Fig. 8 C, D and E show the disagreements among the three forest maps.

1) *MCD12Q1 and GlobCover*. A disagreement between MCD12Q1 and GlobCover was evident (Fig. 8C) as MCD12Q1 has a higher forest area estimate. The 1500 m pixels covered with a significantly smaller percentage of GlobCover-estimated forest than MCD12Q1-estimated forest covered 17% of all the pixels in the study area. 4% of pixels in the study area had over 50% more forest coverage in GlobCover than in MCD12Q1. The remaining 79% of pixels have close forest percentages between GlobCover and MCD12Q1 derived forests. We find that the disagreement between these two datasets is large. Fritz et al. (2011) examined global cropland and forest

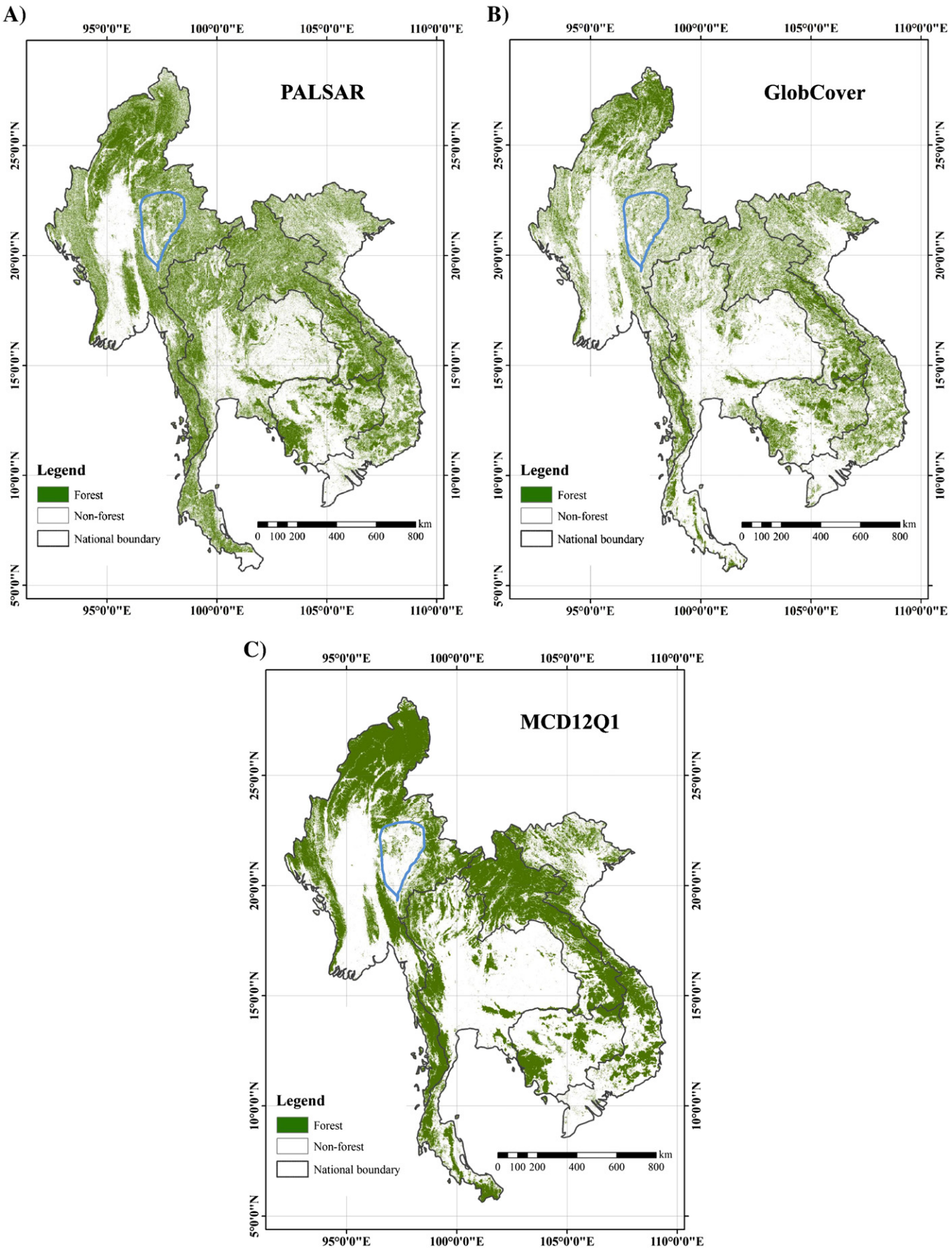

Fig. 7. The spatial distribution of forest from the three datasets in the Mainland Southeast Asia: (A) PALSAR 2009, (B) GlobCover 2009, and (C) MCD12Q1 2009.

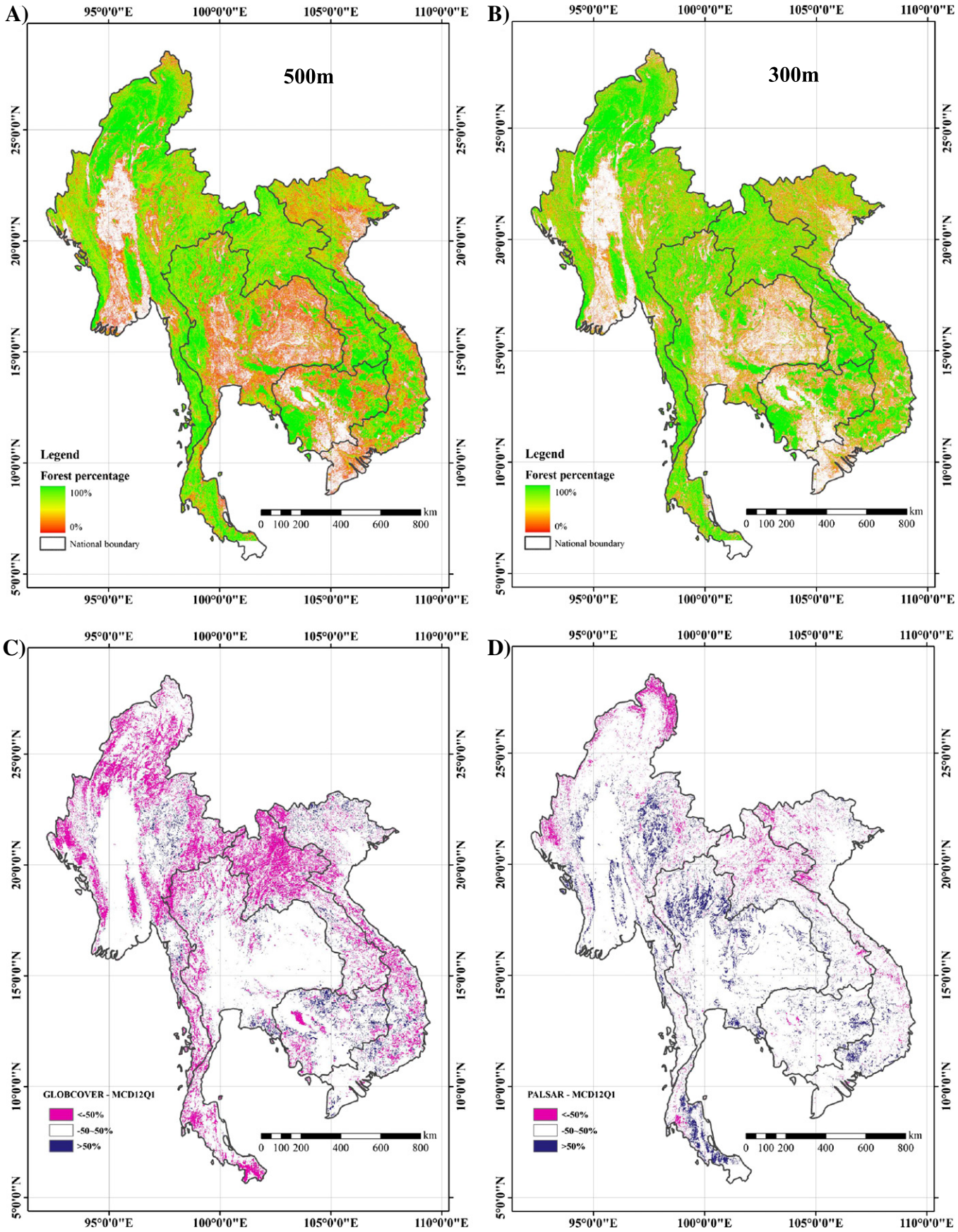

Fig. 8. Forest area percentage maps aggregated from PALSAR 50-m forest map at a resolution of A) 500-m, and B) 300-m; and the disagreement among aggregated 1500-m forest percentage maps of different datasets by pairwise comparison: C) GlobCover and MCD12Q1, D) PALSAR and MCD12Q1, E) PALSAR and GlobCover. The percentage numbers in the legends represent the difference values.

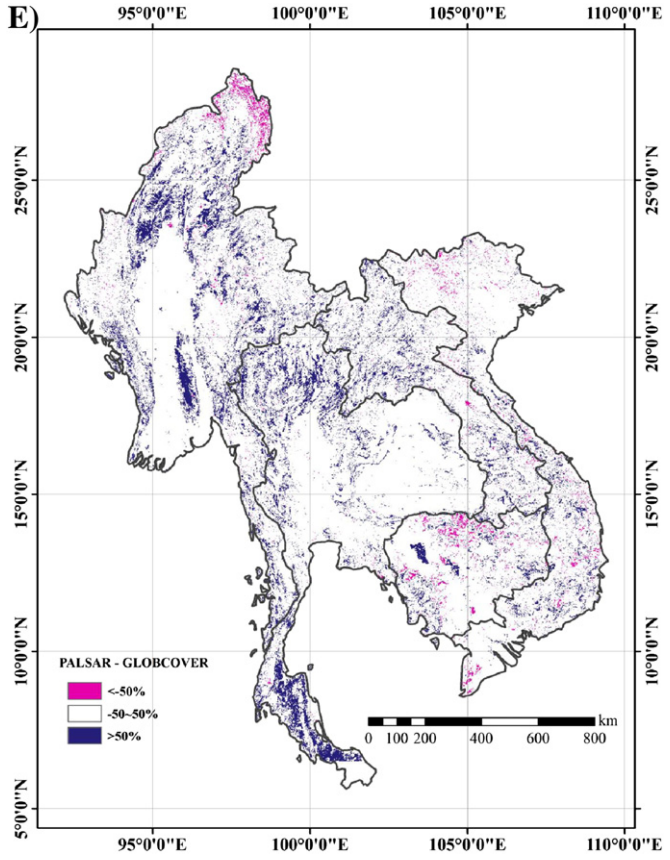

Fig. 8 (*continued*).

disagreement between GlobCover, MCD12Q1, and the Global Land Cover database for the year 2000 (GLC-2000), showing significant uncertainty in these regional/global land cover datasets. Therefore, the application of PALSAR in this study aimed to generate a higher accuracy of forest cover map.

2) *PALSAR and MCD12Q1*. The differences between PALSAR and MCD12Q1 are relatively small compared to the differences between GlobCover and MCD12Q1. Approximately 4% of pixels have a higher forest cover fraction (over 50%) in MCD12Q1 than in the PALSAR derived map, mainly concentrated in the northern hilly regions; while 7% of pixels have a higher forest cover fraction (over 50%) in PALSAR than MCD12Q1, distributed in the southern and northern parts of Thailand, and central-eastern parts of Myanmar.
3) *PALSAR and GlobCover*. Approximately 11% of pixels in the region had a PALSAR forest estimate higher than GlobCover by over 50%, dispersed across the study area (Fig. 8E); the pixels where GlobCover had higher forest fractions (over 50%) covered only 2% and were concentrated in the northern hilly regions. More validation is still needed in these areas. Although we have collected numerous field photos, it is impossible to sample such a large study area completely from the field. The above disagreements could arise from scale issues and variable forest definitions across the different datasets, which is discussed in Section 4.2.

3.4. Assessment of GlobCover and MCD12Q1 forest pixels based on 50-m PALSAR forest cover

We overlaid the fractional forest maps (Fig. 8A, B) from the PALSAR-2009 forest map and the GlobCover 2009 and MCD12Q1 2009 maps, and calculated the percentage of PALSAR forest cover within each GlobCover and MCD12Q1 pixel. The histogram shows that 46% of GlobCover 2009 forest pixels have fractional forest cover > 80%, while 43% of MCD12Q1 2009 forest pixels have fractional forest cover > 80% (Fig. 9). In the FAO FRA 2010 report, 10% tree canopy cover is one criterion for the definition of a forest. Ninety-five percent of forest pixels in the GlobCover 2009 forest map and 98% of forest pixels in the MCD12Q1 2009 forest map have a fractional forest cover > 10%. The comparison results suggest that the forest pixels from GlobCover 2009 and MCD12Q1 2009 have high forest fractions.

To further evaluate the performance of the GlobCover 2009 and MCD12Q1 2009 forest maps and the reliability of the thresholds in the decision tree algorithm, we overlaid the forest maps with PALSAR HH, HV, HH/HV and HH–HV images. We first calculated averages of HH, HV, HH/HV and HH–HV within 300-m pixels and 500-m pixels, and then calculated frequency distributions of HH, HV, HH/HV and HH–HV values for those forest pixels in the GlobCover 2009 and MCD12Q1 2009 datasets (Fig. 10). Fig. 10A shows that for the MCD12Q1 forest map, 95.2% forest pixels were within the HH range (−11 to - 2 dB), 93.2% of forest pixels within the HV range (−15 to −7 dB), 92.1% forest pixels within the HH/HV ratio range (0.3 to 0.7), and 95.6% of forest pixels within HH-HV difference range (4 to 7 dB). These statistics are consistent with those thresholds we used in the decision tree for forest mapping with PALSAR (see Section 2.5). The same situation happens in the forest pixels of the GlobCover 2009 forest map (Fig. 10B) with 92.7% pixels in the HH range (−11 to −2 dB), 87.5% of pixels in the HV range (−15 to −7 dB), 90.5% pixels in the HH/HV range (0.3 to 0.7), and 88.9% of pixels in the HH–HV difference range (4 to 7 dB). This comparison provides additional evidence explaining that the GlobCover 2009 and MCD12Q1 2009 forest pixels have high forest fractions.

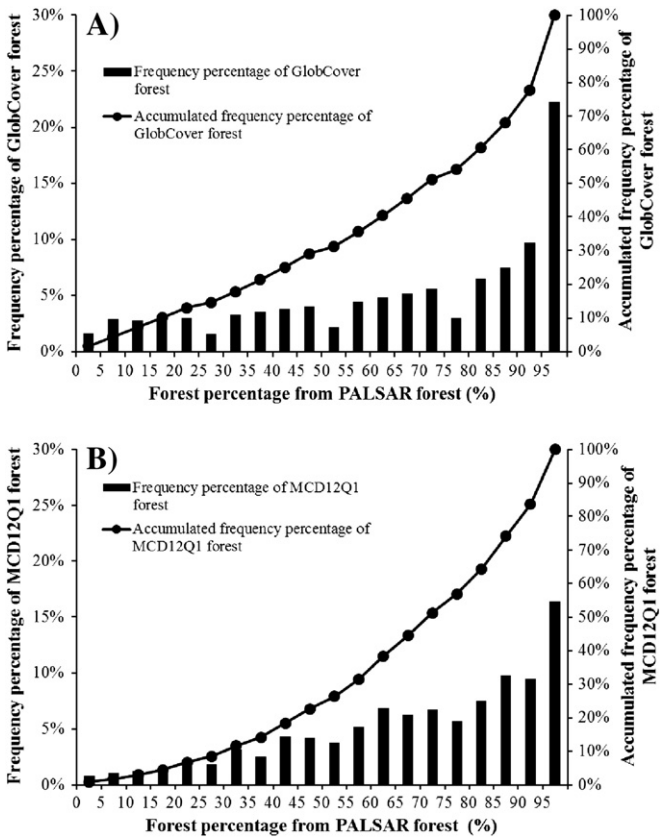

Fig. 9. Frequency histograms of forest area percentages within (A) GlobCover 2009 forest pixels, and (B) MCD12Q1 2009 forest pixels, when these GlobCover and MOCD12Q1 per-pixel forest maps were overlaid with the fractional forest maps aggregated from PALSAR 2009 forest map (50-m resolution).

4. Discussion

4.1. Forest mapping based on PALSAR L-band imagery

The large uncertainty of the forest extent and distribution from recently-published land cover datasets (Fritz et al., 2011) prompted us to pursue a finer resolution forest cover map with higher accuracy, especially in tropical regions (Grainger, 2008). This uncertainty was partly from the frequent cloud cover, which affects forest mapping of humid tropical regions based on optical remote sensing (Asner, 2001; Fritz et al., 2011). The L-band PALSAR sensor provides cloud-free images and its backscatter values are sensitive to vegetation aboveground biomass and structure. The results from several previous studies at the local scale have shown that PALSAR imagery separates forests from other land cover types (Hoekman et al., 2010; Lonnqvist et al., 2010; Lucas et al., 2010, 2007). However, a regional scale forest map based on cloud-free PALSAR imagery was still unavailable to the public prior to this study.

Before PALSAR became available, single HH polarization data from the Japanese Earth Resources Satellite (JERS-1) was widely used for forest mapping (e.g. clear-cut or biomass intensity) in the 1990s (Almeida et al., 2007, 2005; Luckman et al., 1998; Simard et al., 2002); dual polarization (HH, HV) PALSAR images provide improved accuracy in identifying and characterizing forests and deforestation (Almeida et al., 2009; Santoro et al., 2010). In this study, we also evaluated the HH/HV Ratio image and HH–HV Difference image; the HH–HV Difference image proved valuable in identifying and delineating forest, consistent with another study that used PALSAR images to identify woody plantation species (Miettinen & Liew, 2011). A number of algorithms have been developed for mapping forests from L-band SAR images (Santoro et al., 2010; Thiel et al., 2009; Xiao et al., 2010). For example, the support vector machines (SVM) algorithm was used to evaluate the potential of PALSAR orthorectified FBD data at 50-m spatial resolution for identifying forests at a site in Riau Province, Sumatra island, Indonesia (Longepe et al., 2011), and the agreement between the ground reference data and the PALSAR-based natural forest map was 86%. However, a reliable and operational method is necessary for a rapid regional forest mapping. In this study, we developed a simple decision tree algorithm that uses threshold values from HH, HV, HH/HV Ratio and HH–HH Difference images, as a consistent method to map forest, and it performs reasonably well in the area we sampled.

The forest area estimates by country from the PALSAR-based forest map and the FRA 2010 forest estimates have the smallest differences (Fig. 6), this consistency showes the potential of this method for large scale forest inventories. At present, a wall-to-wall forest cover map from the FRA-2010 remote sensing survey is not available to the public. It would be of interest to carry out a spatial comparison between these datasets when the FRA-2010 releases its maps in the near future. If it is in agreement with PALSAR estimates, then this simple and reproducible forest mapping method based PALSAR could positively contribute to forest inventory and management.

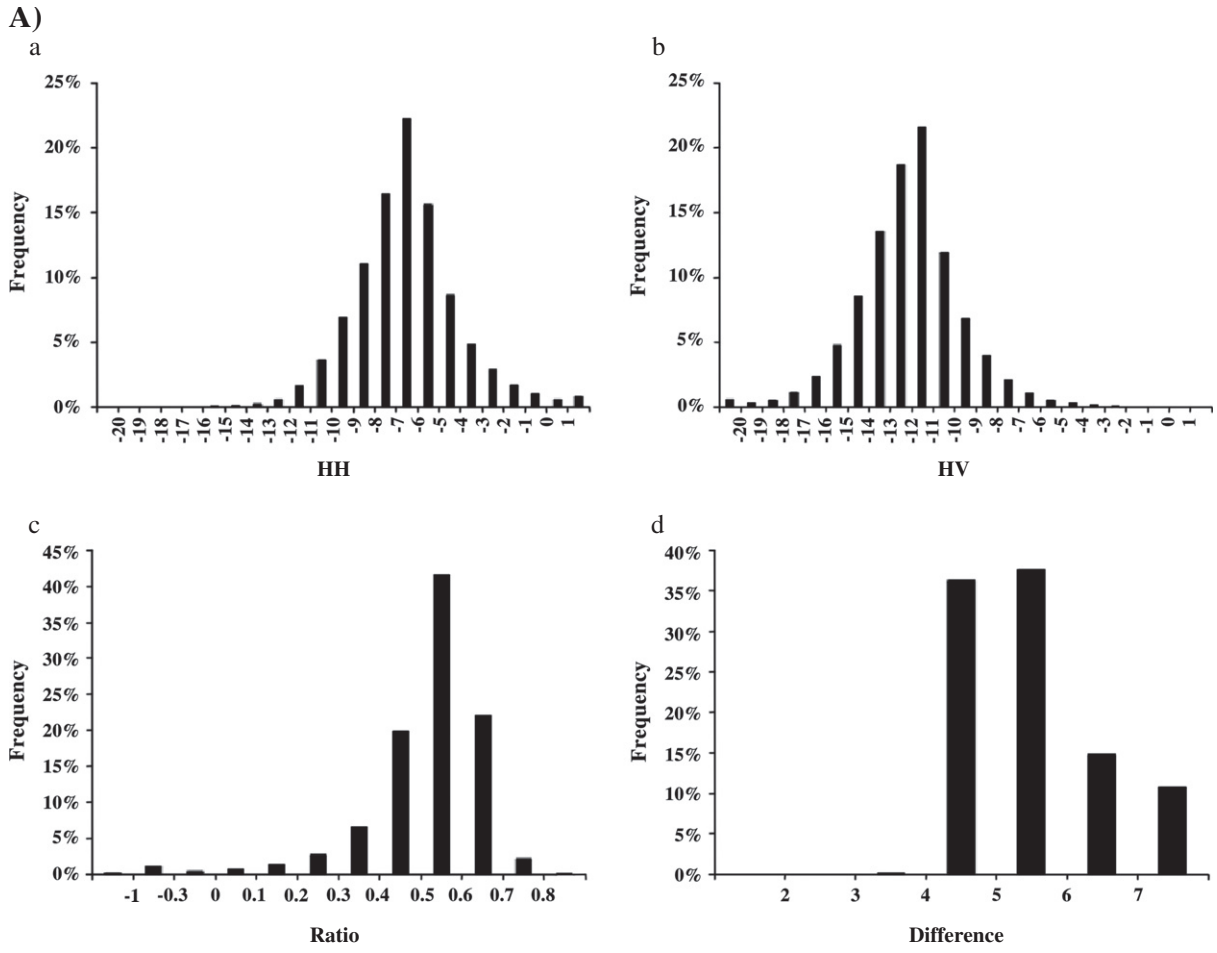

Fig. 10. The polarization signatures within forest pixels of (A) MCD12Q1 2009 forest map and (B) GlobCover 2009 forest map, when these two forest maps were overlaid with backscatter maps of HH, HV, HH/VH, and HH–HV.

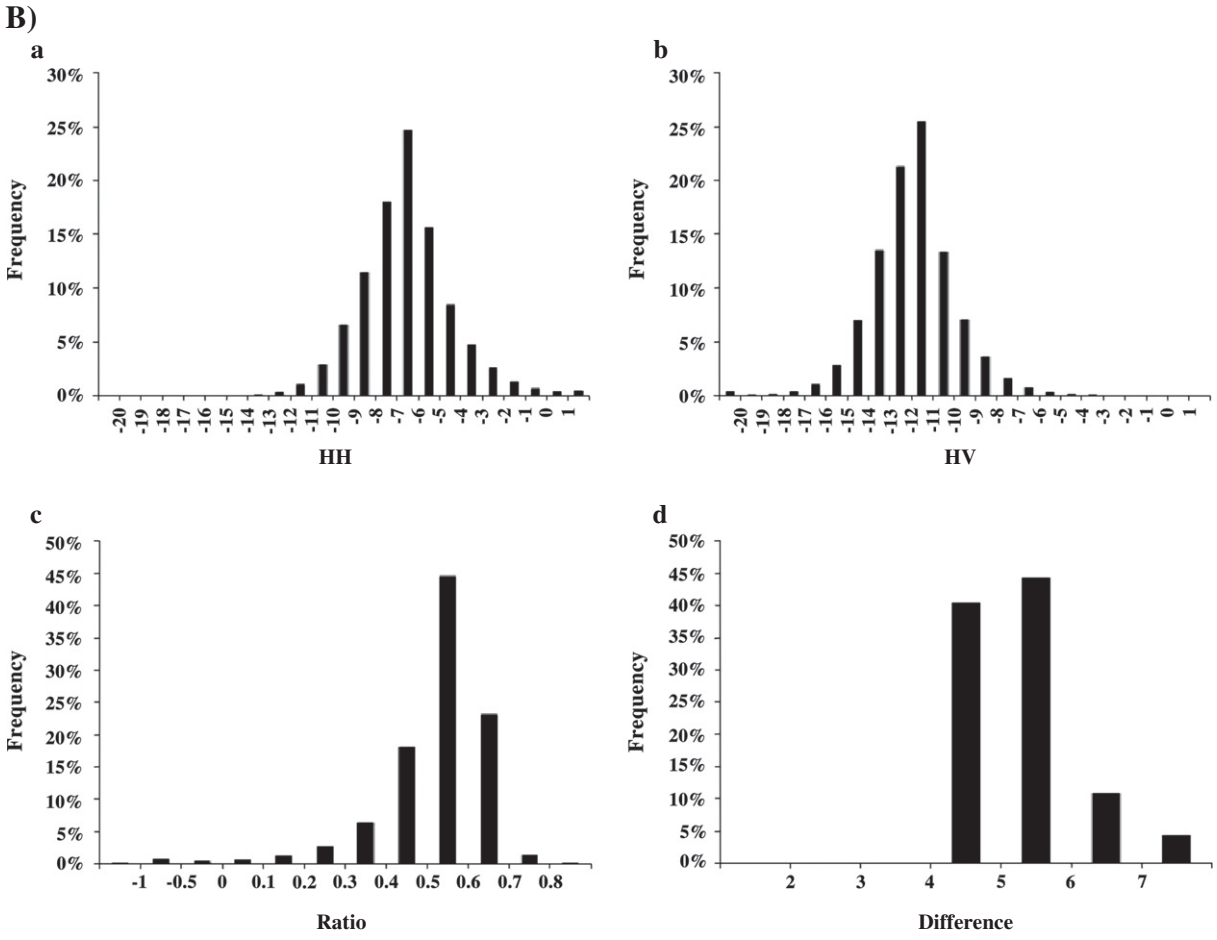

Fig. 10 (*continued*).

4.2. Uncertainty issue

We recognize that the PALSAR forest map generated in this study also has some error and uncertainty, and it could be improved in the future. The first source of uncertainty results from these data being a temporal composite from PALSAR images acquired over the period of July to October in 2009. The backscatter from crops could change in the period that brought some disturbances. Standing crop biomass could increase the radar backscatter coefficient, but post-harvested crop fields (no biomass, or flooded field) could decrease the radar backscatter coefficient. Thus, those pixels with a radar backscatter coefficient at the border of the decision tree threshold values could be misclassified at different periods.

The second source of uncertainty is the definition of forest and its characteristic signature in remote sensing images. According to the definition from FAO, forest refers to a land parcel (0.5 ha or larger) with a tree canopy cover of more than 10% and tree height of 5 m and up (FAO, 2001). Forests are defined by the presence of trees and the absence of other predominant land uses (FAO, 2001). Open and closed forests were further defined by tree canopy cover (Achard et al., 2002). Our study used the FAO definition, which could be one reason that our result is close to FAO, 2010. It might be more reasonable to take advantage of the higher resolution PALSAR and produce the forest map at the resolution with the smallest forest unit according to the FAO definition. However, these two factors (% tree canopy cover and tree height) are difficult to accurately measure by moderate resolution optical and SAR remote sensing. Although a pixel of the PALSAR 50-m orthorectified mosaic imagery is smaller than the minimum unit area (0.5 ha or ~70 m × 70 m) for the FAO forest definition, it's still difficult to acquire tree canopy cover, as the radar backscatter coefficient is an integrated indicator affected by a series of complex factors. The pixel sizes in the GlobCover 2009 and MCD12Q1 2009 datasets are much larger than the minimum unit area for forest as defined by FAO, and accordingly, the issue of mixing pixels might be more severe. MCD12Q1 and GlobCover applied different forest definitions (Bontemps et al., 2011; Strahler et al., 1999), e.g., 15% was used as bottom limit of the tree canopy cover in GlobCover while MCD12Q1 used 60%; in addition, GlobCover used the same tree height threshold (5 m) as FAO while 2 m is used in MCD12Q1. The area disagreements among the three datasets are partly from the sub-forest categories in different land cover classification schemes (Table 3) (Bontemps et al., 2011; FAO, 2001; Friedl et al., 2010). For example, in the FAO FRA 2010 Report, forest areas exclude those with agricultural purposes or urban development. It is currently almost impossible to distinguish forest use type (forestry use or agricultural use) by remote sensing. In the GlobCover 2009 classification system, some classes are a mixed type with two or more vegetation types, e.g. the type of "mosaic vegetation (grassland/shrubland/forest) (50–70%) / cropland (20–50%)." Minimum forest patch depends on the pixel size to a large extent.

The third source of uncertainty comes from complexity of landscapes in MSEA, driven by complex topography and intensive agricultural practice (e.g., terrace crop fields, mixed cropping). Although several studies have also evaluated the potential of PALSAR 50-m orthorectified mosaic data in identifying different forest types (Miettinen & Liew, 2011; Thiel et al., 2009; Xiao et al., 2010), more complicated forest type classification methods are less robust than a simple forest/non-forest classification (Walker et al., 2010), as the

overall accuracy decreased when more and varied forest types were considered. The diverse and complex landscapes suggest that future study is needed to gather more ground reference data (e.g., geo-referenced field photos) and improve characterization of signatures for individual forest types.

4.3. Implication and future work

The results of this study have demonstrated the potential of PALSAR 50-m orthorectified mosaic imagery for regional-scale mapping of forest. As JAXA has already released PALSAR 50-m mosaic imagery for Southeast Asia and tropical Africa to the public and is planning to release PALSAR 50-m mosaic imagery for South America, it is possible to develop PALSAR-based tropical forest maps across the pan-tropical zone using the approach described in this study. Work is ongoing to map the pan-tropical forest cover based on ALOS image mosaic data by WHRC/ the Alaska Satellite Facility (Kellndorfer, 2010). The JERS-1 SAR images (HH) over the Amazon, Central America, equatorial Africa and Southeast Asia were mosaicked with some 13 000 SAR scenes for large scale of applications (Rosenqvist et al., 2000; Shimada et al., 2000) and are freely available. Although JERS-1 single polarization imagery has some shortcomings in forest delineation (Santoro et al., 2010), it is a valuable data source for forest change analysis. A study on forest change in Southeast Asia between 1990s (JERS-1 imagery available in 1996) and 2009 (PALSAR) could provide invaluable information on deforestation in the region. As MSEA has undergone huge forest changes in recent past, deforestation and afforestation were concurrent (FAO, 2010). In addition, including texture information in classification in the future could improve estimates, as the texture can help in separation between natural forest and plantation which have different shapes.

5. Conclusion

There is large variability across tropical forest area estimates for 2009–2010 from multispectral optical remote sensing and the FAO FRA forest estimates in Mainland Southeast Asia. The forest map produced from 2009 PALSAR 50-m orthorectified mosaic imagery in this study indicates better accuracy in forest estimates due to both the higher spatial resolution and cloud-free observation of the PALSAR imagery. The use of PALSAR to estimate forest allows for the evaluation of forest area estimates derived from multispectral data and other statistical methods, something which until now has proven challenging. If the accuracy of forest cover estimates using PALSAR radar imagery is consistent across other tropical regions, then estimates of tropical forest area across the globe can be obtained with greater accuracy using these data. The PALSAR-based forest cover map could provide a reference for forest inventory and also perform as a background map to support ecological modeling.

Acknowledgments

This study was supported by the NASA Land Use and Land Cover Change program (NNX09AC39G, NNX11AJ35G) and the USA National Science Foundation (NSF) EPSCoR program (NSF-0919466). The PALSAR 50 m orthorectified mosaic data are provided by JAXA as the ALOS sample product. The authors would like to thank the Editor Dr. Scott Goetz and four anonymous reviewers for their valuable suggestions and comments on the earlier version of this manuscript, which help us substantially for revision of the manuscript.

References

Achard, F., & Estreguil, C. (1995). Forest classification of Southeast Asia using NOAA AVHRR data. *Remote Sensing of Environment*, *54*, 198–208.

Achard, F., Eva, H., & Mayaux, P. (2001). Tropical forest mapping from coarse spatial resolution satellite data: Production and accuracy assessment issues. *International Journal of Remote Sensing*, *22*, 2741–2762.

Achard, F., Eva, H. D., Stibig, H. J., Mayaux, P., Gallego, J., Richards, T., et al. (2002). Determination of deforestation rates of the world's humid tropical forests. *Science*, *297*, 999–1002.

Agrawal, A., Chhatre, A., & Hardin, R. (2008). Changing governance of the world's forests. *Science*, *320*, 1460–1462.

Almeida, R., Rosenqvist, A., Shimabukuro, Y. E., & Silva-Gomez, R. (2007). Detecting deforestation with multitemporal L-band SAR imagery: A case study in western Brazilian Amazonia. *International Journal of Remote Sensing*, *28*, 1383–1390.

Almeida, R., Roskenqvist, A., Shimabukuro, Y. E., & dos Santos, J. R. (2005). Evaluation and perspectives of using multitemporal L-band SAR data to monitor deforestation in the Brazilian Amazonia. *IEEE Geoscience and Remote Sensing Letters*, *2*, 409–412.

Almeida, R., Shimabukuro, Y. E., Rosenqvist, A., & Sanchez, G. A. (2009). Using dual-polarized ALOS PALSAR data for detecting new fronts of deforestation in the Brazilian Amazonia. *International Journal of Remote Sensing*, *30*, 3735–3743.

Asner, G. P. (2001). Cloud cover in Landsat observations of the Brazilian Amazon. *International Journal of Remote Sensing*, *22*, 3855–3862.

Baghdadi, N., Boyer, N., Todoroff, P., El Hajj, M., & Begue, A. (2009). Potential of SAR sensors TerraSAR-X, ASAR/ENVISAT and PALSAR/ALOS for monitoring sugarcane crops on Reunion Island. *Remote Sensing of Environment*, *113*, 1724–1738.

Benedek, C., & Sziranyi, T. (2009). Change detection in optical aerial images by a multilayer conditional mixed Markov model. *IEEE Transactions on Geoscience and Remote Sensing*, *47*, 3416–3430.

Bontemps, S., Defourny, P., Van Bogaert, Eric, Arino, O., Kalogirou, V., & Perez, J. R. (2011). *GLOBCOVER 2009: Products description and validation report.*

Chazdon, R. L. (2008). Beyond deforestation: Restoring forests and ecosystem services on degraded lands. *Science*, *320*, 1458–1460.

Cohen, W. B., Yang, Z. G., & Kennedy, R. (2010). Detecting trends in forest disturbance and recovery using yearly Landsat time series: 2. TimeSync - Tools for calibration and validation. *Remote Sensing of Environment*, *114*, 2911–2924.

Curran, L. M. (2004). Lowland forest loss in protected areas of Indonesian Borneo. *Science*, *303*, 1000–1003.

Dechert, G., Veldkamp, E., & Anas, I. (2004). Is soil degradation unrelated to deforestation? Examining soil parameters of land use systems in upland Central Sulawesi, Indonesia. *Plant and Soil*, *265*, 197–209.

FAO (2001). *FAO FRA 2000 — Main report. Rome.*

FAO (2010). *Global forest resources assessment 2010. Rome.*

FAO, JRC, SDSU, & UCL (2009). The 2010 global forest resources assessment remote sensing survey: An outline of the objectives, data, methods and approach. *Forest resources assessment working paper*, *155*, Rome: FAO with FRA RSS partners.

Fearnside, P. M. (2000). Global warming and tropical land-use change: Greenhouse gas emissions from biomass burning, decomposition and soils in forest conversion, shifting cultivation and secondary vegetation. *Climatic Change*, *46*, 115–158.

Friedl, M. A., Sulla-Menashe, D., Tan, B., Schneider, A., Ramankutty, N., Sibley, A., et al. (2010). MODIS collection 5 global land cover: Algorithm refinements and characterization of new datasets. *Remote Sensing of Environment*, *114*, 168–182.

Fritz, S., See, L., McCallum, I., Schill, C., Obersteiner, M., van der Velde, M., et al. (2011). Highlighting continued uncertainty in global land cover maps for the user community. *Environmental Research Letters*, *6*, 044005.

Gemmell, A. L., Smith, G. C., Haines, K., & Blower, J. D. (2009). Validation of ocean model syntheses against hydrography using a new web application. *Journal of Operational Oceanography*, *2*, 29–41.

Giri, C., Defourny, P., & Shrestha, S. (2003). Land cover characterization and mapping of continental Southeast Asia using multi-resolution satellite sensor data. *International Journal of Remote Sensing*, *24*, 4181–4196.

Grainger, A. (2008). Difficulties in tracking the long-term global trend in tropical forest area. *Proceedings of the National Academy of Sciences of the United States of America*, *105*, 818–823.

Grainger, A. (2010). Uncertainty in the construction of global knowledge of tropical forests. *Progress in Physical Geography*, *34*, 811–844.

Hansen, M. C., Stehman, S. V., & Potapov, P. V. (2010a). Quantification of global gross forest cover loss. *Proceedings of the National Academy of Sciences of the United States of America*, *107*, 8650–8655.

Hansen, M. C., Stehman, S. V., & Potapov, P. V. (2010b). Reply to Wernick et al.: Global scale quantification of forest change. *Proceedings of the National Academy of Sciences of the United States of America*, *107*, E148-E148.

Hansen, M. C., Stehman, S. V., Potapov, P. V., Loveland, T. R., Townshend, J. R. G., DeFries, R. S., et al. (2008). Humid tropical forest clearing from 2000 to 2005 quantified by using multitemporal and multiresolution remotely sensed data. *Proceedings of the National Academy of Sciences of the United States of America*, *105*, 9439–9444.

Hoekman, D. H., Vissers, M. A. M., & Wielaard, N. (2010). PALSAR Wide-Area Mapping of Borneo: Methodology and map validation. *IEEE Journal of Selected Topics in Applied Earth Observations and Remote Sensing*, *3*, 605–617.

JAXA-EORC (2010). Generation of global forest/non-forest map using ALOS/PALSAR. *JAXA EORC*.

Kaptue Tchuente, A. T., Roujean, J. L., & De Jong, S. M. (2011). Comparison and relative quality assessment of the GLC2000, GLOBCOVER, MODIS and ECOCLIMAP land cover data sets at the African continental scale. *International Journal of Applied Earth Observation and Geoinformation*, *13*, 207–219.

Kellndorfer, J. (2010). Pan-tropical forest cover mapped with cloud-free radar imaging. [In]. http://www.whrc.org/mapping/pantropical/alos.html

Langner, A., Miettinen, J., & Siegert, F. (2007). Land cover change 2002–2005 in Borneo and the role of fire derived from MODIS imagery. *Global Change Biology*, *13*, 2329–2340.

Lawton, J. H., Bignell, D. E., Bolton, B., Bloemers, G. F., Eggleton, P., Hammond, P. M., et al. (1998). Biodiversity inventories, indicator taxa and effects of habitat modification in tropical forest. *Nature*, *391*, 72–76.

Longepe, N., Rakwatin, P., Isoguchi, O., Shimada, M., Uryu, Y., & Yulianto, K. (2011). Assessment of ALOS PALSAR 50 m orthorectified FBD data for regional land cover classification by support vector machines. *IEEE Transactions on Geoscience and Remote Sensing*, *49*, 2135–2150.

Lonnqvist, A., Rauste, Y., Molinier, M., & Hame, T. (2010). Polarimetric SAR data in land cover mapping in Boreal zone. *IEEE Transactions on Geoscience and Remote Sensing*, *48*, 3652–3662.

Lucas, R., Armston, J., Fairfax, R., Fensham, R., Accad, A., Carreiras, J., et al. (2010). An evaluation of the ALOS PALSAR L-band backscatter-above ground biomass relationship Queensland, Australia: Impacts of surface moisture condition and vegetation structure. *IEEE Journal of Selected Topics in Applied Earth Observations and Remote Sensing*, *3*, 576–593.

Lucas, R. M., Mitchell, A. L., Rosenqvist, A., Proisy, C., Melius, A., & Ticehurst, C. (2007). The potential of L-band SAR for quantifying mangrove characteristics and change: case studies from the tropics. *Aquatic Conservation: Marine and Freshwater Ecosystems*, *17*, 245–264.

Luckman, A., Baker, J., Honzak, M., & Lucas, R. (1998). Tropical forest biomass density estimation using JERS-1 SAR: Seasonal variation, confidence limits, and application to image mosaics. *Remote Sensing of Environment*, *63*, 126–139.

Meijaard, E., & Sheil, D. (2007). A logged forest in Borneo is better than none at all. *Nature*, *446*, 974-974.

Miettinen, J. (2007). Variability of fire-induced changes in MODIS surface reflectance by land-cover type in Borneo. *International Journal of Remote Sensing*, *28*, 4967–4984.

Miettinen, J., & Liew, S. C. (2011). Separability of insular Southeast Asian woody plantation species in the 50 m resolution ALOS PALSAR mosaic product. *Remote Sensing Letters*, *2*, 299–307.

Miettinen, J., Shi, C. H., & Liew, S. C. (2011). Deforestation rates in insular Southeast Asia between 2000 and 2010. *Global Change Biology*, *17*, 2261–2270.

Miettinen, J., Shi, C., Tan, W. J., & Chinliew, S. (2012). 2010 land cover map of insular Southeast Asia in 250-m spatial resolution. *Remote Sensing Letters*, *3*, 11–20.

Montesano, P. M., Nelson, R., Sun, G., Margolis, H., Kerber, A., & Ranson, K. J. (2009). MODIS tree cover validation for the circumpolar taiga-tundra transition zone. *Remote Sensing of Environment*, *113*, 2130–2141.

Pimm, S. L., & Raven, P. (2000). Biodiversity — Extinction by numbers. *Nature*, *403*, 843–845.

Potere, D. (2008). Horizontal positional accuracy of Google Earth's high-resolution imagery archive. *Sensors*, *8*, 7973–7981.

Rosenqvist, A., Shimada, M., Chapman, B., Freeman, A., De Grandi, G., Saatchi, S., et al. (2000). The global rain forest mapping project — A review. *International Journal of Remote Sensing*, *21*, 1375–1387.

Rosenqvist, A., Shimada, M., Ito, N., & Watanabe, M. (2007). ALOS PALSAR: A pathfinder mission for global-scale monitoring of the environment. *IEEE Transactions on Geoscience and Remote Sensing*, *45*, 3307–3316.

Salati, E., & Nobre, C. A. (1991). Possible climatic impacts of tropical deforestation. *Climatic Change*, *19*, 177–196.

Santoro, M., Fransson, J. E. S., Eriksson, L. E. B., & Ulander, L. M. H. (2010). Clear-cut detection in Swedish boreal forest using multi-temporal ALOS PALSAR backscatter data. *IEEE Journal of Selected Topics in Applied Earth Observations and Remote Sensing*, *3*, 618–631.

Shimada, M., Isoguchi, O., & Rosenqvist, A. (2008). Palsar Calval and generation of the continent scale mosaic products for Kyoto and carbon projects. *Geoscience and remote sensing symposium, 2008. IGARSS 2008. IEEE International*. (pp. I-17–I-20).

Shimada, M., & Ohtaki, T. (2010). Generating large-scale high-quality SAR mosaic datasets: Application to PALSAR data for global monitoring. *IEEE Journal of Selected Topics in Applied Earth Observations and Remote Sensing*, *3*, 637–656.

Shimada, M., Wakabayashi, H., Tadono, T., Isoguchi, O., & Miyagawa, H. (2000). JERS-1 SAR mosaics over the Southeast Asia. *Geoscience and Remote Sensing Symposium, 2000. Proceedings. IGARSS 2000. IEEE 2000 International*, *vol.1*. (pp. 1–3).

Simard, M., De Grandi, G., Saatchi, S., & Mayaux, P. (2002). Mapping tropical coastal vegetation using JERS-1 and ERS-1 radar data with a decision tree classifier. *International Journal of Remote Sensing*, *23*, 1461–1474.

Stibig, H. J., Achard, F., & Fritz, S. (2004). A new forest cover map of continental southeast Asia derived from SPOT-VEGETATION satellite imagery. *Applied Vegetation Science*, *7*, 153–162.

Stibig, H. J., & Malingreau, J. P. (2003). Forest cover of insular southeast Asia mapped from recent satellite images of coarse spatial resolution. *Ambio*, *32*, 469–475.

Strahler, A., Muchoney, D., Borak, J., Friedl, M., Gopal, S., Lambin, E., et al. (1999). MODIS land cover product algorithm theoretical basis document (ATBD) version 5.0. Boston: Boston University.

Thiel, C. J., Thiel, C., & Schmullius, C. C. (2009). Operational large-area forest monitoring in Siberia using ALOS PALSAR summer intensities and winter coherence. *IEEE Transactions on Geoscience and Remote Sensing*, *47*, 3993–4000.

Tottrup, C., Rasmussen, M. S., Eklundh, L., & Jonsson, P. (2007). Mapping fractional forest cover across the highlands of mainland Southeast Asia using MODIS data and regression tree modelling. *International Journal of Remote Sensing*, *28*, 23–46.

UNEP/GRID-Arendal (2009). *Vital forest graphics*. Nairobi, Kenya: UNEP.

Walker, W. S., Stickler, C. M., Kellndorfer, J. M., Kirsch, K. M., & Nepstad, D. C. (2010). Large-area classification and mapping of forest and land cover in the Brazilian Amazon: A comparative analysis of ALOS/PALSAR and Landsat data sources. *IEEE Journal of Selected Topics in Applied Earth Observations and Remote Sensing*, *3*, 594–604.

Wu, F., Wang, C., Zhang, H., Zhang, B., & Tang, Y. X. (2011). Rice crop monitoring in South China With RADARSAT-2 quad-polarization SAR data. *IEEE Geoscience and Remote Sensing Letters*, *8*, 196–200.

Wurster, C. M., Bird, M. I., Bull, I. D., Creed, F., Bryant, C., Dungait, J. A. J., et al. (2010). Forest contraction in north equatorial Southeast Asia during the Last Glacial Period. *Proceedings of the National Academy of Sciences of the United States of America*, *107*, 15508–15511.

Xiao, X., Biradar, C., Czarnecki, C., Alabi, T., & Keller, M. (2009). A simple algorithm for large-scale mapping of evergreen forests in tropical America, Africa and Asia. *Remote Sensing*, *1*, 355–374.

Xiao, X., Dorovskoy, P., Biradar, C., & Bridge, E. (2011). A library of georeferenced photos from the field. *EOS. Transactions of the American Geophysical Union*, *92*.

Xiao, W., Wang, X., & Ling, F. (2010). The application of ALOS PALSAR data on mangrove forest extraction. *Remote Sensing Technology and Application*, *25*, 91–96.